CHAPTER V
NON-OXIDATIVE METHANE REFORMING IN AN AC GLIDING ARC MICROREACTOR: EFFECTS OF OPERATIONAL PARAMETERS AND THE PRESENCE OF CATALYST*

5.1 Abstract

In this investigation, a non-thermal plasma microreactor generating a gliding arc discharge was employed for directly converting methane to various products. Acetylene and hydrogen were dominantly produced at ambient temperature and atmospheric pressure, with high selectivities of ~70–90% and ~75%, respectively. Small amounts of other products — including ethylene, ethane, butadiene, and carbon residue — were also formed. The results showed that both methane conversion and product selectivities strongly depended on various operational parameters, namely input power, discharge gap between electrodes, reactor width, and feed flow rate. A Ni-loaded porous alumina–silica catalyst plate, prepared by the wet impregnation method, was used to explore the catalytic effect with varying residence times. A considerable enhancement of methane conversion and product yields was achieved in the combined plasma–catalyst system, particularly at a longer residence time. The distance between the catalyst and plasma zone of microreactor configuration was also found to be an influential factor in promoting the combined plasma-catalytic non-oxidative methane reforming. The closer distance resulted in greater methane conversion because of more possibilities for the adsorption–desorption interactions of excited gaseous species on the catalyst surface to enhance subsequent reactions. Furthermore, the temperature effect on the surface of the Ni-loaded catalyst brought about a significant change in product selectivities.

---

*Being Prepared for International Journal of Plasma Environmental Science & Technology

Keywords: Methane conversion; Non-thermal plasma; Gliding arc discharge; Microreactor

5.2 Introduction

Natural gas is the cleanest and environmentally-safest primary fossil fuel in terms of its lowest emission of CO_2. Interestingly, numerous investigations have been reportedly focused on the upgrading conversion process of methane (CH_4), which is a main constituent in natural gas in all vast reserves around the world to produce higher value-added chemicals instead. The use of non-thermal plasma is a direct method for many chemical conversion processes, also involving either the non-oxidative methane reforming [1-7], the oxidative methane reforming [8-13], or the hybrid plasma-catalytic reforming of methane [14-19]. Due to its non-equilibrium property, non-thermal plasma with high-energy electrons create principally a large number of chemically active species through electronic and ionic collision processes, and then immediately induce the subsequent chemical reactions under room temperature and atmospheric pressure. Hence, highly-stable methane molecules can be potentially converted by means of non-thermal plasma. For further development of the non-thermal plasma processing, some researchers have integrated it with the novel idea of microreactor technology [20-25]. In a microreactor, its extremely small volume and large specific surface area significantly provide several process improvements, such as the better heat distribution and heat transfer, the precise control of a shorter residence time, and the small processing amounts of reactants [20-27].

Herein, this research focused on studying the production of useful chemicals (higher hydrocarbons and hydrogen) from direct non-oxidative methane conversion by using gliding arc discharge, a new discharge type of non-thermal plasma, together with the microreactor technology concept. For the first experimental part, the effects of electrical parameters, including input power, discharge gap, reactor width, and feed flow rate, on the non-oxidative methane reforming were investigated. For the second part, the effect of nickel metal loaded on a porous alumina-silica catalyst plate on the performance of the non-oxidative methane reforming was studied, for

the first time, with varying residence time. The nickel-loaded catalyst was chosen in the present study, due to the common reasons of its availability and cost-effectiveness. Moreover, the heating effect of the catalyst surface on the reaction performance was also studied.

5.3 Experimental

5.3.1 Gliding Arc Microreactor System

The configuration of the gliding arc discharge microreactor and the experimental set-up of the studied plasma system are illustrated in Figures 5.1 and 5.2, respectively. The gliding arc discharge microreactor was made of two glass plates with a width of 7 cm, a length of 10 cm, and a thickness of 0.5 cm, and had two diverging knife-shaped electrodes fabricated from two stainless steel sheets with a thickness of 0.25 mm. These electrodes were vertically positioned inside the reactor and connected to the power supply. The gap distance between the electrode pairs was adjustable. Two pre-drilled holes on the glass cover (reactor wall) served as an inlet and outlet gas lines. Two teflon sheets with different thicknesses were placed between the reactor glass walls and the electrodes on both sides (see Figure 5.1(a)), to create various reactor volumes, and also to seal up the microreactor. Additionally, to examine the effect of catalyst in this studied plasma microreactor system, a catalyst plate with 2x3 cm^2 in size was inserted into the middle of a holder of silicone rubber sheet, and then was packed between the reactor glass wall and the teflon sheet on the back side of the microreactor (see Figure 5.1(b)) in order to locate the catalyst close to the plasma zone without any interference to the plasma characteristics and the flow pattern. For the experiments to study the effect of catalyst surface temperature, the catalyst plate was heated up to 210°C by being externally irradiated with an infrared (IR) beam equipped with a halogen lamp (LCB50) and an IR beam heater (LCB-PS12, Inflidge Industrial Ltd.). The temperature on the surface of catalyst plate was determined by using a thermal label indicator.

In this study, a mixed feed gas having 5% CH_4 with Ar balance was introduced upward to the gliding arc microreactor system. The flow rates of CH_4 and

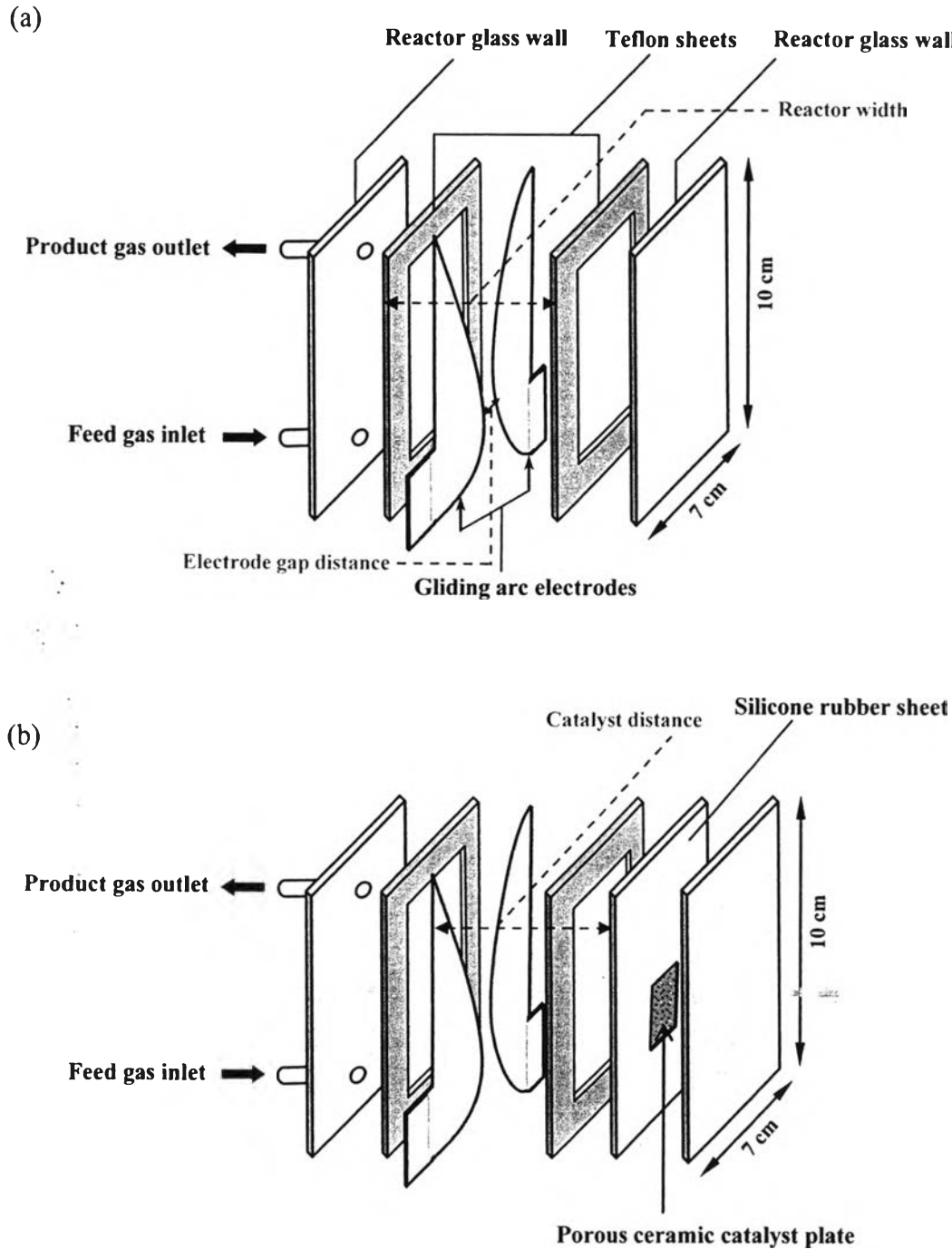

Figure 5.1 Configuration of a gliding arc discharge microreactor (a) in the absence of catalyst and (b) in the presence of catalyst.

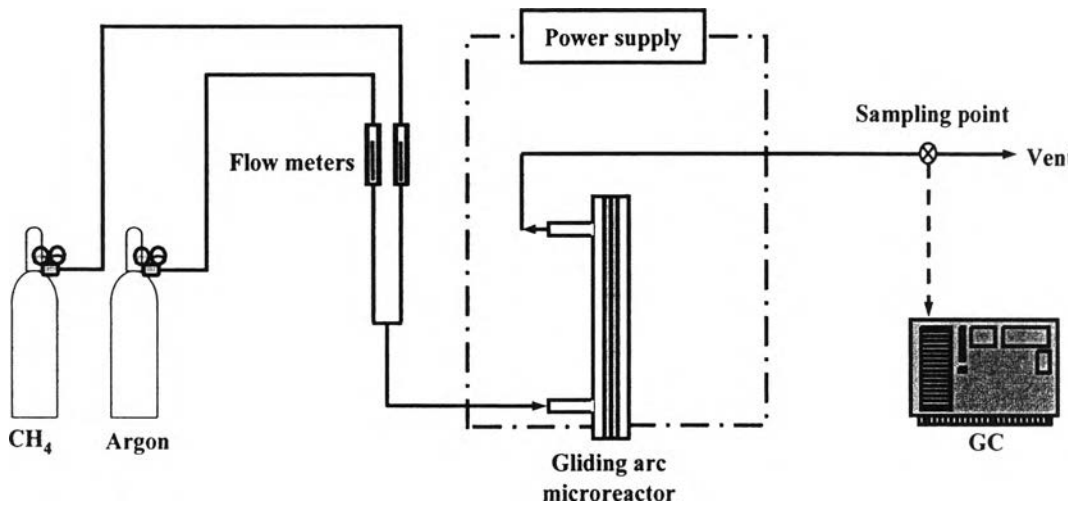

Figure 5.2 Experimental set-up of the gliding arc plasma system.

Ar were regulated by flowmeters. After the composition of feed gas was invariant with time, the power unit was turned on. An AC high frequency power supply system (Alpha Neon, M-5) with a maximum voltage of 9 kV was applied to the plasma microreactor to generate the gliding arc discharge. The input power was controlled by a step-up variable transformer. After the system reached equilibrium state (normally within 3 min after turning the power on), an analysis of outlet gas composition was taken at least a few times. The experimental data were averaged to assess the process performance. The compositions of the feed gas stream and the product gas stream were analyzed by two gas chromatographs. The first gas chromatograph (Shimadzu, GC-14B) equipped with a GS-GasPro capillary column and a flame ionization detector (FID) was used to detect CH_4, C_2H_2, C_2H_4, C_2H_6, and butadiene (1,3-C_4H_6). The second one (Shimadzu, GC-8A) equipped with a molecular sieve 13X packed column and a thermal conductivity detector (TCD) was used to detect H_2. A digital power meter was used to measure input power, current, and voltage at the low voltage side of the power supply unit. The discharge waveforms of current and voltage were observed by an oscilloscope (Tektronix, TDS 1012 B). For the combined plasma and catalyst system, the experiment was repeated at least three times, in order to ensure the reproducibility of the experimental data. The experimental conditions used in this study are summarized in Table 5.1.

Table 5.1 Experimental conditions used in this study

Operational parameter	Operating value
Input power	4-12 W
Electrode gap distance	2-5 mm
Reactor width	0.65-4.25 mm
Feed flow rate	75, 100, and 200 cm^3/min
Catalyst distance	0.2 and 0.5 mm

5.3.2 Catalyst Preparation and Characterizations

The porous ceramic plate with a chemical composition of 23% SiO_2, 75% Al_2O_3, and 2% others used as a catalyst support was supplied by Nikkato Corporation. The BET specific surface area and the specific pore volume of the catalyst support were 2.6 m^2/g and 5.9 mm^3/g, respectively, as determined by a surface area analyzer (Thermo Finnigan, Sorptomatic 1990). $Ni(NO_3)_2 \cdot 6H_2O$ with 98% purity obtained from Wako Pure Chemical Industries, Ltd. was used as a nickel precursor. To prepare the nickel loaded on the catalyst support by the wet impregnation method, the porous silica-alumina plate was immersed in an aqueous solution of 2.0 M $Ni(NO_3)_2 \cdot 6H_2O$ for 10 h. After that, the catalyst was dried at 110°C for 2 h, and then calcined in air at 500°C for 5 h. The amount of Ni loading was approximately 5 wt.%. The calcined catalyst was further reduced in a H_2 (25% H_2 in Ar balance) flowing at 200 cm^3/min in a quartz tube with an inner diameter of 2.5 cm. The quartz tube was heated by a cylindrical furnace at 500°C for 3 h. The prepared catalyst was characterized by an X-ray diffractometer (XRD) system (Rigaku/Rint, 2200HV) and a scanning electron microscope (SEM, JEOL, JSM-6400) equipped with an energy dispersive X-ray analyzer (EDX, Link ISIS, Series 300).

5.3.3 Reaction Performance Assessment

The methane conversion is defined as:

$$\% \text{ Methane conversion} = \frac{(\text{moles of methane } in - \text{moles of methane } out)\,(100)}{\text{moles of methane } in} \quad (5.1)$$

Note that the total flow rate of outlet gas and the amount of carbon solid (C) are calculated from the C and H atomic mass balances.

$$\% \text{ Selectivity for any hydrocarbon product} = \frac{(\text{amount of C atoms in the hydrocarbon product})(100)}{\Sigma\,(\text{amount of C atoms in the C-containing products})} \quad (5.2)$$

$$\% \text{ Selectivity for hydrogen} = \frac{(\text{amount of H atoms in the hydrogen product})(100)}{\Sigma\,(\text{amount of H atoms in the H-containing products})} \quad (5.3)$$

The product yields are formulated as follows:

$$\%\ C_2 \text{ hydrocarbon yield} = (\%\ CH_4 \text{ conversion})\ \Sigma\ (\%\ C_2H_2, C_2H_4, C_2H_6 \text{ selectivity}) / (100) \quad (5.4)$$

$$\%\ H_2 \text{ yield} = (\%\ CH_4 \text{ conversion})\ (\%\ H_2 \text{ selectivity}) / (100) \quad (5.5)$$

5.4 Results and Discussion

5.4.1 Catalyst Characterization Results

XRD spectra of the porous silica-alumina catalyst plate without and with nickel loading are comparatively shown in Figure 5.3. For the unloaded catalyst

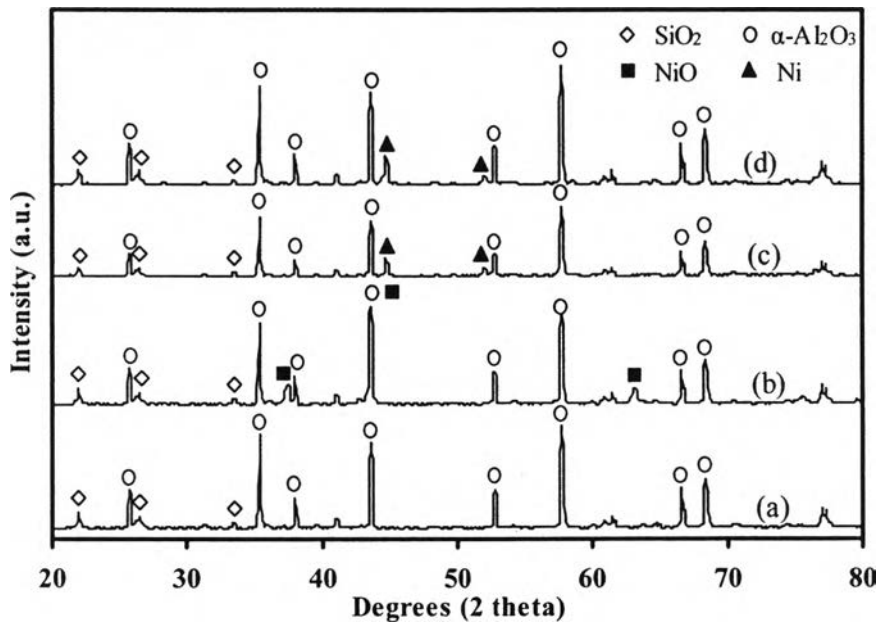

Figure 5.3 XRD patterns of (a) unloaded catalyst plate (silica-alumina support), (b) calcined NiO-loaded catalyst plate, (c) reduced Ni-loaded catalyst plate, (d) spent Ni-loaded catalyst plate.

plate in Figure 5.3(a), the SiO_2 and α-Al_2O_3 were observed as two major crystalline phases. For the catalyst plate with nickel loading, the NiO phase was appeared as indicated by the diffraction peaks at 37.5° and 66.7° after the calcination treatment, as shown in Figure 5.3(b), but, the NiO phase completely changed to the Ni phase indicated by the diffraction peaks at 44.7° and 52.1° when it was reduced in H_2 atmosphere, as shown in Figure 5.3(c). The Ni phase was still found in the spent catalyst plate (after the plasma reaction), as shown in Figure 5.3(d). In a comparison of the metal crystallite size between before and after the plasma reaction, the Ni crystallite sizes calculated from Scherrer formula were nearly the same (about 28.87 and 26.60 nm for the reduced Ni-loaded catalyst and spent Ni-loaded catalyst plates, respectively). Figure 5.4 shows the typical SEM micrograph and EDX mappings of the Ni-loaded catalyst plate. The pore structure of the porous silica-alumina plate can be clearly observed. From the elemental distributions, the Ni species were found to be highly dispersed on the surface of silica-alumina plate, verifying that the prepared catalyst plates contained uniform Ni distribution.

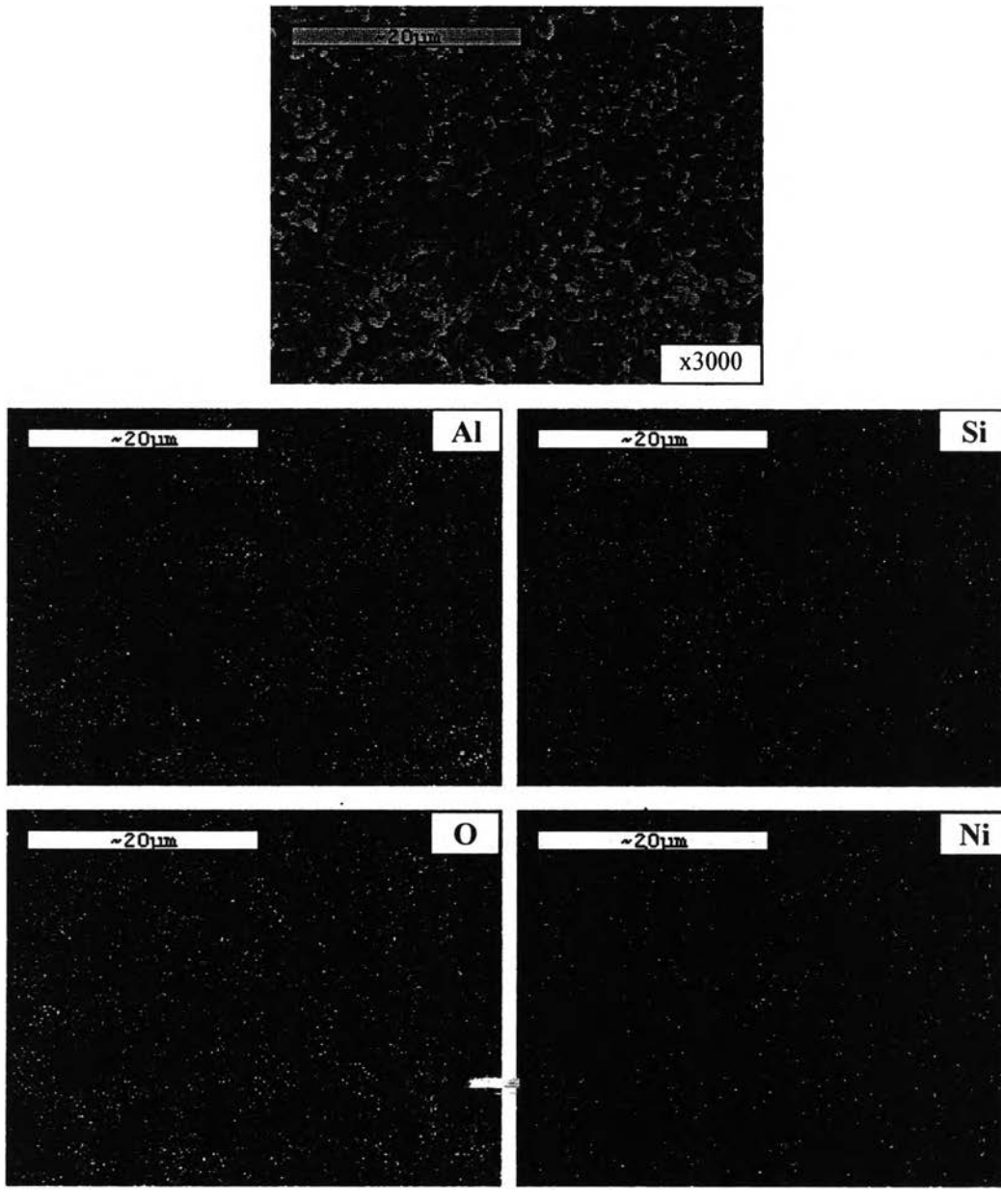

Figure 5.4 Typical SEM micrograph and EDX area mappings of the Ni-loaded catalyst plate.

5.4.2 Effect of Input Power

The input power is technically regarded as a key parameter in operating the plasma chemical processing and in sustaining the plasma stability. To investigate the influence of input power on the non-oxidative methane reforming under the gliding arc microreactor system, the input power was experimentally varied in the range of 4-12 W, while the feed flow rate, electrode gap distance, and

reactor width between the reactor glass walls were kept constant. In this gliding arc system, the lowest operating input power of 4 W was the minimum value of input power required to initiate the plasma generation with the steady plasma environment, whereas the highest operating input power of 12 W was due to the limitation of the studied power supply unit. Figure 5.5(a) shows the results of methane conversion and product yields as a function of input power. The methane conversion and the yields of H_2 and C_2 hydrocarbon products increased with increasing input power. For any given input power, the C_2 yield was higher than the H_2 yield, and their difference tended to increase with increasing input power. In fact, a higher input power gives a direct effect on a greater energy supplied to the plasma system, which can provide not only electrons with a higher average energy and temperature but also a higher electron density. These generated electrons have more ability to break down the strong C-H bond of methane, thereby leading to an increasing methane conversion.

From the results of product distribution (Figure 5.5(b)), the dominant products from direct methane conversion under the gliding arc discharge environment were C_2H_2 and H_2, with their high selectivities of ~70-90% and ~75%, respectively. Other products (C_2H_4, C_2H_6, and C_4H_6) were also detected, but with relatively low levels. Interestingly, under the studied conditions, C_3 and higher hydrocarbons were not detected, suggesting that the studied gliding arc microreactor is not efficient in producing higher hydrocarbons from non-oxidative methane reforming. Besides, significant amount of coke (carbon residue) was found to deposit on the inner reactor glass wall and electrode surface close to the high temperature region of gliding arc discharge. An increase in input power tended to decrease the selectivities for all C_2 hydrocarbons and carbon whereas the H_2 selectivity remained unchanged. It is clearly seen that the main products of C_2H_2 and H_2) tended to be produced rather than larger hydrocarbons. The excitation thresholds for generating CH_3, CH_2, CH, and C species formed from the direct electron impact dissociation of CH_4 are ca. 9.0, 10.0, 11.0, and 12.0 eV, respectively [12]. From the approximation of the energy supplied to this studied plasma system, the energy per a molecule of CH_4 introduced was estimated to be up to 18.2 eV, in the investigated range of input power. These imply that the average electron energy level in the studied gliding arc discharge is sufficiently high enough to dissociate methane molecules into all

species; with CH as the major methyl species among CH_3, CH_2, and CH, due to a large amount of C_2H_2 formed as the main product, as above explained. Therefore, C_2H_2 can be consecutively formed by the coupling reaction of CH radicals (CH + CH $\rightarrow$ C_2H_2).

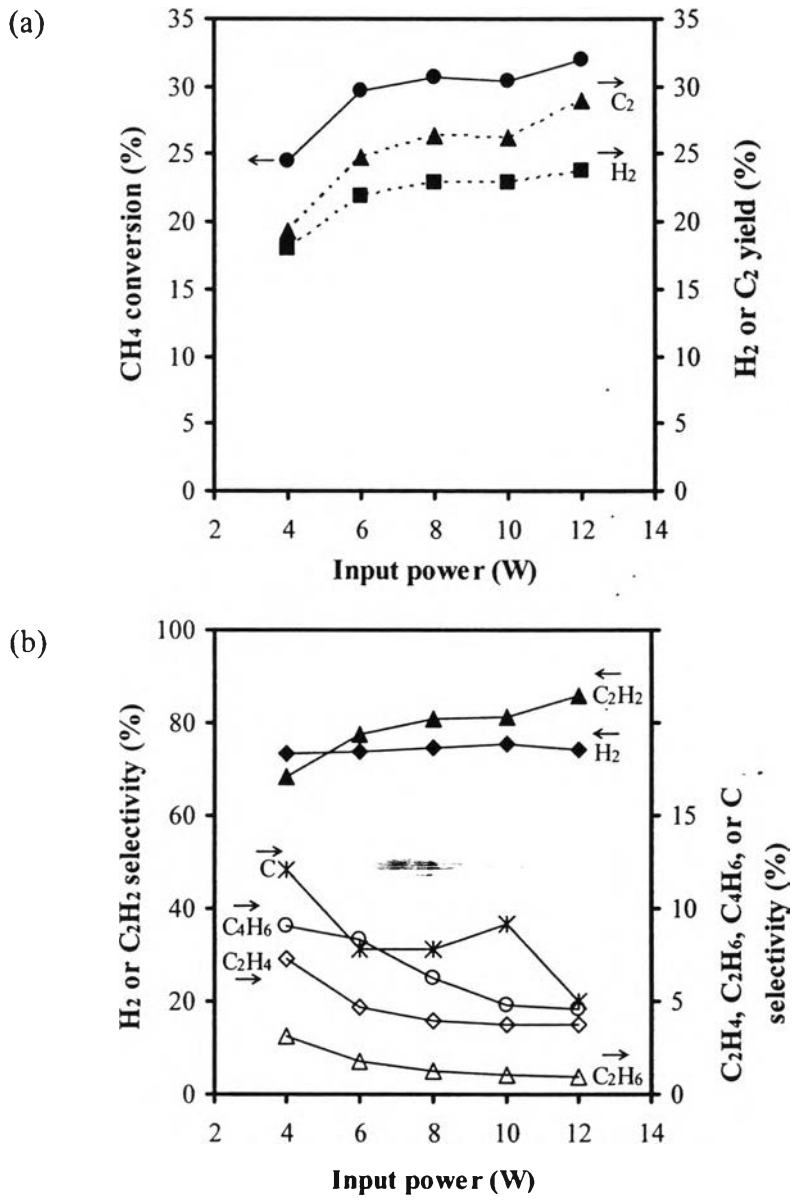

Figure 5.5 Effect of input power on (a) methane conversion and product yields, and (b) product selectivities of the non-oxidative methane reforming (CH_4 in feed, 5%; feed flow rate, 200 cm^3/min; electrode gap distance, 4 mm; and, reactor width, 1.25 mm).

5.4.3 Effect of Electrode Gap Distance

With the diverging knife-shaped electrode geometry of the studied gliding arc plasma reactor, the electrode gap distance represents the narrowest gap distance between the two electrodes, where the arc discharge is initially generated. Changing gap distance between the electrodes — in other words, discharge gap distance — affects both the electric field strength, the residence time, and subsequently the plasma reactions. Figure 5.6 shows the effect of electrode gap distance on the reaction performance, with varying electrode gap distance between 2–5 mm. Under the studied conditions, the plasma system could not be operated at the electrode gap distance below 2 mm due to a tremendous amount of coke filament forming between the two electrodes within a short operation time, causing permanent extinction of the plasma. The electrode gap distance of 5 mm was a maximum value in capable of generating the steady plasma environment at a constant input power of 6 W. Interestingly, it can be clearly seen from Figure 5.6(a) that the methane conversion and product yields remarkably increase as the gap distance of electrodes is increased. The results can be explained in that with increasing electrode gap distance (from 2 to 5 mm), the electric field strength across the electrodes was weaker or the average electron energy was lower due to lower operating voltage observed (from 61.20 to 48.85 V) at a constant input power, causing the negative effect on methane conversion; however, the residence time was longer (from 0.026 to 0.049 s) due to the largely increased reaction volume, leading to the positive effect on methane conversion. The results of increasing methane conversion and yields with increasing electrode gap distance suggest that the positive effect of longer residence time essentially dominates over the negative effect of weaker electric field strength.

Figure 5.6(b) shows the effect of electrode gap distance on the product selectivities. It was experimentally found that the selectivities for H_2, C_2H_2, C_2H_4, and C_2H_6 were hardly affected by the electrode gap distance. However, the C_4H_6 selectivity increased when the electrode gap distance was gradually increased, but the C selectivity decreased. It is believed that the longer residence time when increasing electrode gap distance plays a major role in the enhancement of C_4H_6 formation, the largest hydrocarbon molecule found in this system. For the C

selectivity, the tendency of carbon formation was higher at a narrower electrode gap distance, because the increasing strength of electric generates the electrons in plasma field having higher energy, leading to increasing the methane cracking reaction ($CH_4 \rightarrow C + 2H_2$), despite a shorter residence time.

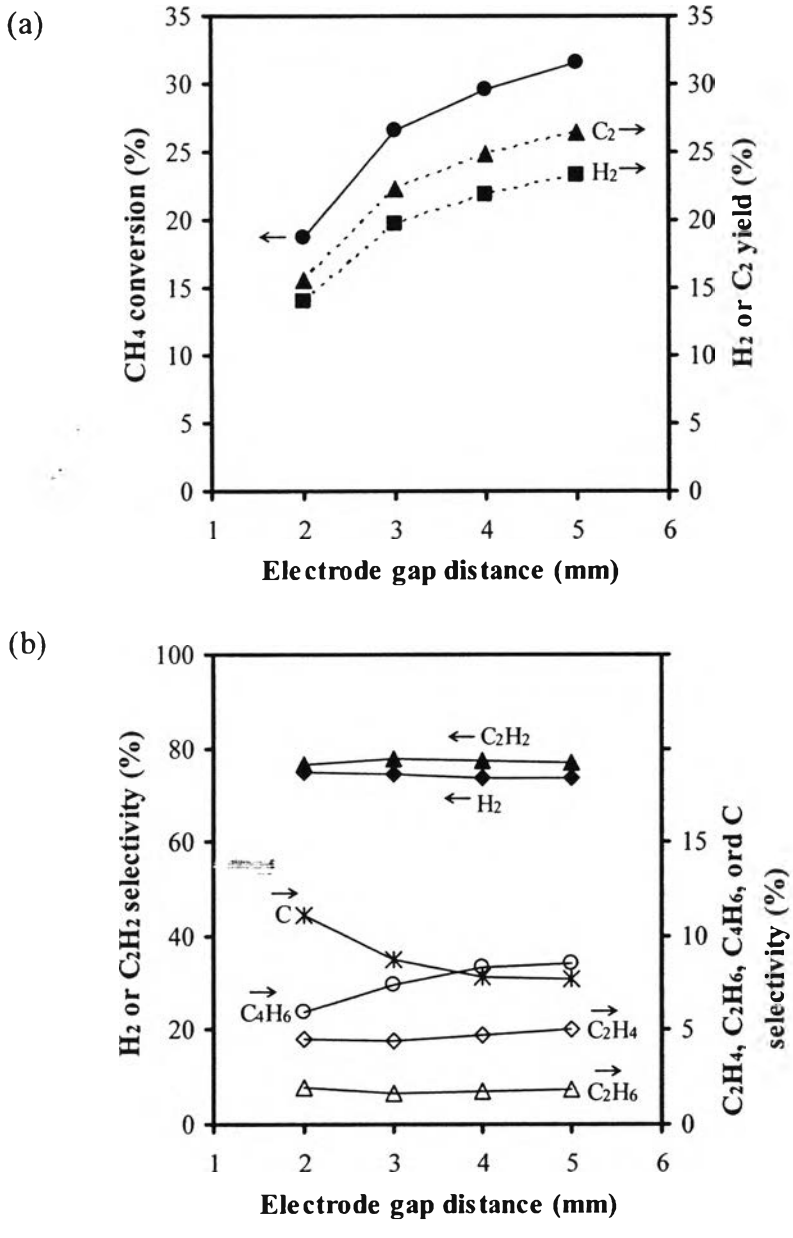

Figure 5.6 Effect of electrode gap distance on (a) methane conversion and product yields, and (b) product selectivities of the non-oxidative methane reforming (CH_4 in feed, 5%; feed flow rate, 200 cm^3/min; input power, 6 W; and, reactor width, 1.25 mm).

5.4.4 Effect of Reactor Width

The main goal for investigating the effect of reactor width was to determine how the heat-transfer characteristics of the microreactor impact the reaction performance under the non-thermal gliding arc discharge. The reactor width was varied by changing the thickness of the teflon sheet from 0.2 to 0.5, 1.0, 1.5, and 2.0 mm, which corresponded to the reactor widths of 0.65, 1.25, 2.25, 3.25, and 4.25 mm, respectively (see Figure 5.7). It must be noted that the teflon sheet thickness less than 0.2 mm was not used due to the geometry limitation of the plasma microreactor used in this study. In the microreactor, the smaller the reactor width, the higher surface area-to-volume ratio of plasma zone, therefore resulting in the easier and more uniform heat-transfer rate from the plasma generated between electrodes to the reactor glass walls. Additionally, the residence time is proportionally changed with the reactor width or the reaction volume within the microreactor, by noting that the residence time, t, is calculated from the ratio of the reaction volume, V, and total feed flow rate, Q ($t = V/Q$). Hence, the smaller the reactor width, the shorter the residence time. Figure 5.7(a) shows the significant increases in both methane conversion and product yields with increasing reactor width. A possible explanation for this result is that, when the reactor width is increased, the residence time increases, resulting in obtaining more opportunity of electron-CH_4 collisions. The result suggests that this positive effect is clearly predominant to the negative effect of less heat transfer of plasma on the reaction performance.

In terms of product distribution, the effect of reactor width on the selectivities for H_2, C_2H_2, C_2H_4, C_2H_6, C_4H_6, and C is shown in Figure 5.7(b). The H_2 and C_4H_6 selectivities remained almost unchanged throughout the investigated range of reactor width. However, when increasing reactor width from 0.65 to 1.25 mm, the selectivities for C_2H_4, C_2H_6, and C slightly dropped. After that, upon further increasing reactor width beyond 1.25 mm, the C selectivity turned to radically increase, whereas the selectivities for C_2H_4 and C_2H_6 only slightly increased. In the meantime, the C_2H_2 selectivity exhibited the opposite trend to the C selectivity. For the reactor width range of 0.65-1.25 mm, the increase in C_2H_4, C_2H_6 and C selectivities at the narrower reactor width may result from the influences of higher surface area-to-volume ratio of the plasma zone and therefore the better heat transfer

(a)

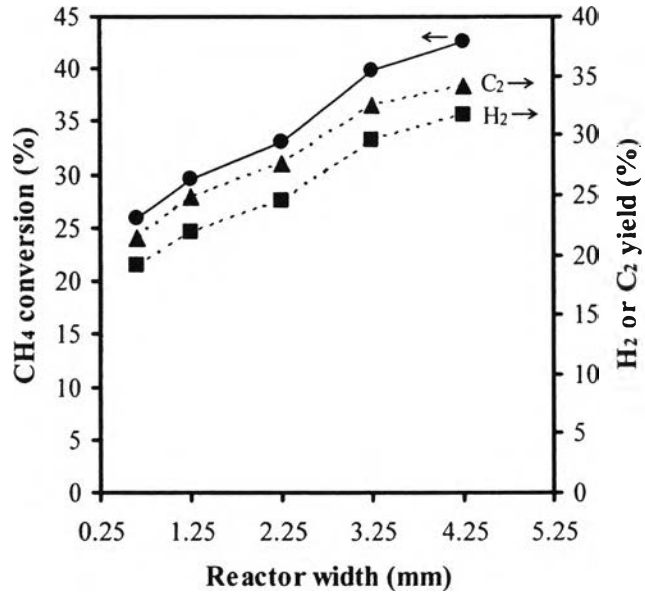

(b)

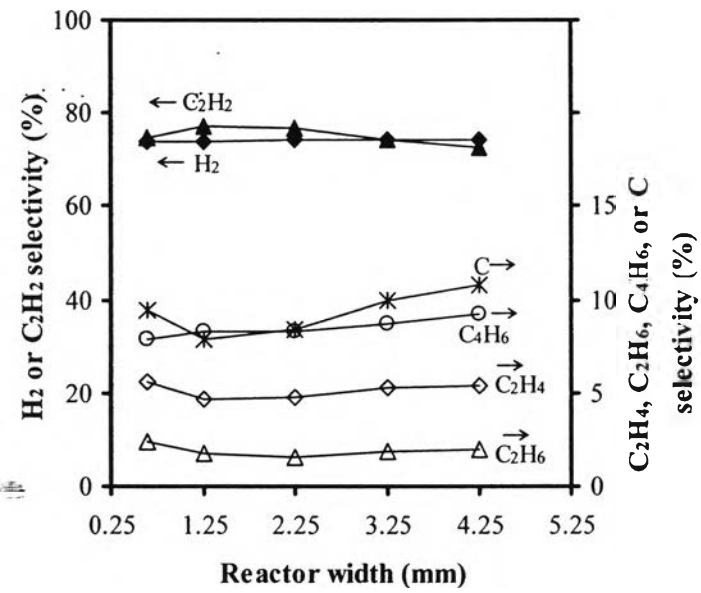

Figure 5.7 Effect of reactor width on (a) methane conversion and product yields, and (b) product selectivities of the non-oxidative methane reforming (CH_4 in feed, 5%; feed flow rate, 200 cm^3/min; input power, 6 W; and, electrode gap distance, 4 mm).

between plasma and reactor walls in the microreactor. However, for the reactor width range of 1.25-4.25 mm, the increase in those selectivities, in particular C selectivity, at the larger reactor width may be caused by the increase in residence time, which plays a more important role in the reaction performance at a higher reactor width.

The position of catalyst in the plasma reactor may affect the reaction pathways. Thus, the catalyst plate had to be placed close to the plasma zone while avoiding the interference of the plasma generation and the flow pattern. From the obtained results of the reactor width effect, a reactor width of 1.25 mm provided the reasonably high performance in terms of both the maximum C_2H_2 selectivity and the minimum C selectivity, even though the greater methane conversion and product yields could be achieved at the larger reactor widths. Therefore, the reactor width of 1.25 mm was selected for the further study of the combined plasma-catalytic non-oxidative methane reforming.

5.4.5 Effect of the Presence of Catalyst

For the investigation of the combined plasma-catalytic non-oxidative reforming of methane under ambient conditions, three systems of plasma alone, plasma+unloaded catalyst, and plasma+Ni-loaded catalyst were performed by changing the feed flow rate between 75-100 cm^3/min at two catalyst distances of 0.2 mm (residence time: 0.03-0.08 s) and 0.5 mm (residence time: 0.04-0.11 s), which in overall corresponded to a variation of residence time in the range of 0.03-0.11 s. The effects of the presence of catalyst on methane conversion, product yields, and product selectivities are shown in Figures 5.8-5.10. As described before (the effects of electrode gap and reactor width), the residence time is regarded as a dominant factor affecting the methane conversion in this gliding arc discharge microreactor. Therefore, the performance of various systems was compared based on the same residence time. As expected, for both the absence of catalyst (plasma alone) and the presence of unloaded and Ni-loaded porous silica-alumina catalyst plates, increasing residence time resulted in the significant enhancement of methane conversion. For any given catalyst distance, the presence of unloaded and Ni-loaded catalysts in the plasma system led to a synergistic effect in improving the methane conversion, as compared to the sole plasma system. Especially, there are more noticeable differences in methane conversion among those systems at higher residence times. The best result was found in the plasma+Ni-loaded catalyst system, of which the highest methane conversion greater than 50% was obtained at a feed flow rate of 75 cm^3/min and a catalyst distance of 0.2 mm (0.08 s residence time). The increasing

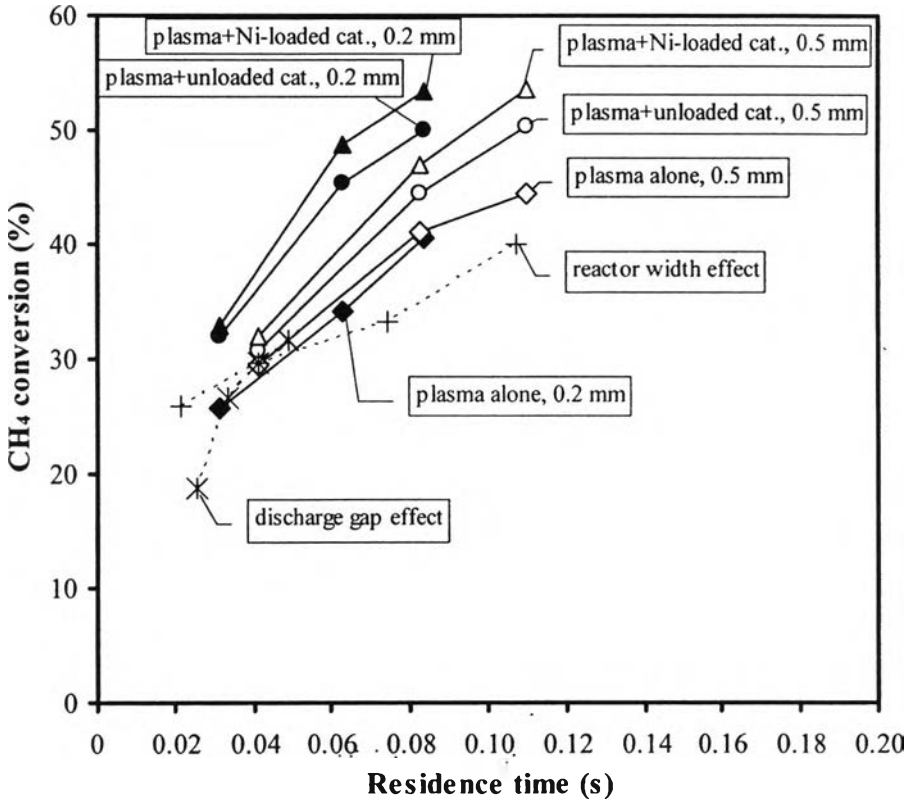

Figure 5.8 Effect of the presence of catalyst on methane conversion of the combined catalytic-plasma non-oxidative methane reforming (solid symbol: catalyst distance of 0.2 mm, open symbol: catalyst distance of 0.5 mm) (CH_4 in feed, 5%; electrode gap distance, 4 mm; and input power, 6 W).

methane conversion under the combined plasma-catalyst system results from the higher adsorption and desorption capabilities of plasma-excited species [14]. Interestingly, when considering the reaction performance at the same residence, the results of catalyst distance effect (0.2 and 0.5 mm) showed that the methane conversion increased with decreasing catalyst distance in both the plasma+unloaded catalyst and plasma+Ni-loaded catalyst systems were obtained. This indicates that the distance between catalyst and plasma zone has a great influence on the adsorption-desorption characteristics of excited gaseous species on the catalyst surface. The closer the catalyst distance, the higher the possibilities of excited gaseous species adsorbed on the catalyst surface, leading to the enhancement of subsequent reactions. In the case of system with plasma alone, for any fixed residence time, the methane conversion at the catalyst distance of 0.5 mm was

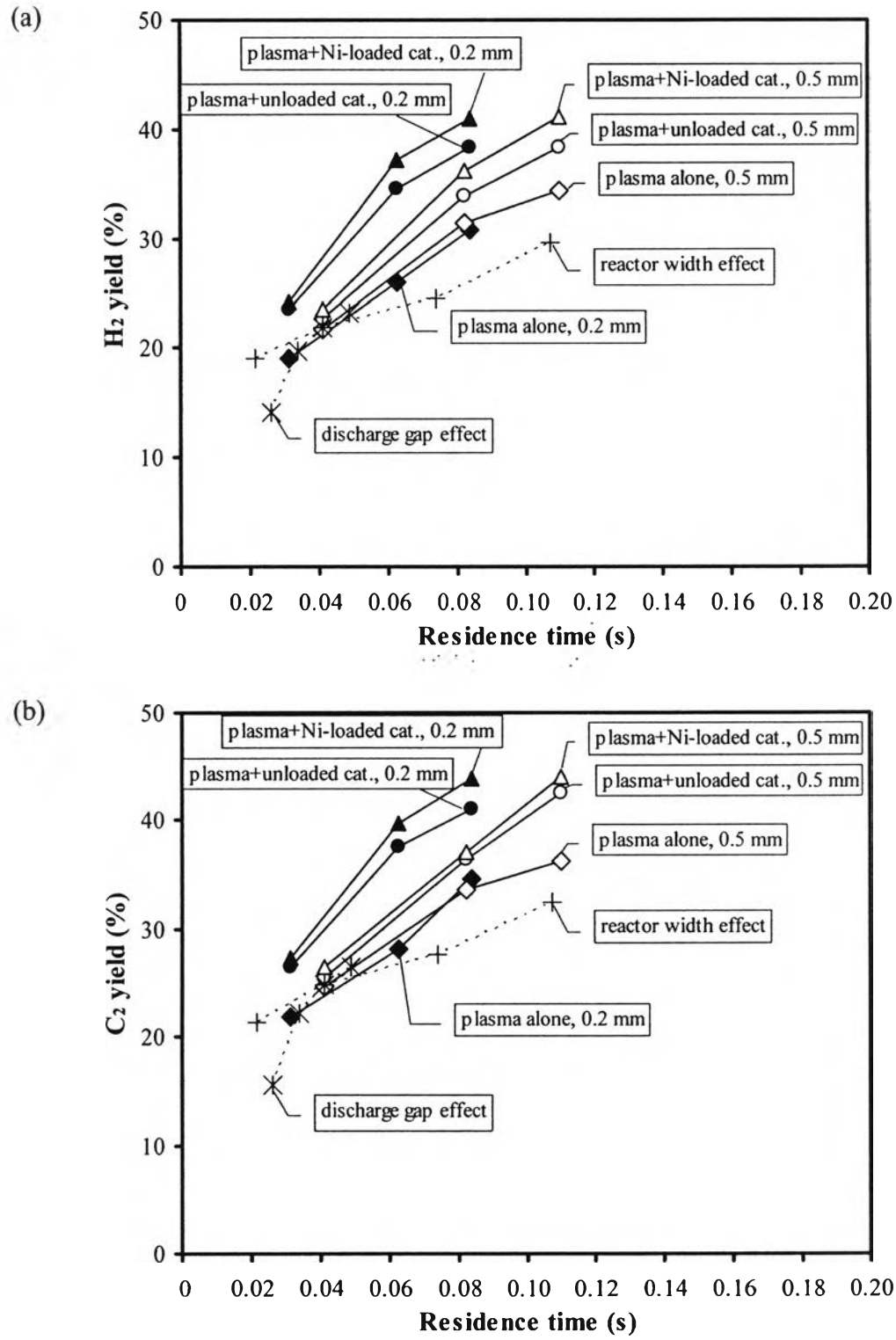

Figure 5.9 Effect of the presence of catalyst on (a) H_2 yield and (b) C_2 yield of the combined catalytic-plasma non-oxidative methane reforming (solid symbol: catalyst distance of 0.2 mm, open symbol: catalyst distance of 0.5 mm) (CH_4 in feed, 5%; electrode gap distance, 4 mm; and input power, 6 W).

slightly higher than that at the catalyst distance of 0.2 mm, indicating that the geometric configuration had a little effect on the methane conversion. As shown in Figure 5.9, the product yields of H_2 and C_2 have the similar trends to the methane conversion. However, for the comparative results of C_2 yield in the two cases between the plasma+unloaded catalyst and the plasma+Ni-loaded catalyst systems at the catalyst distance of 0.5 mm (see Figure 5.9(b)), a very slight difference in C_2 yield between two systems was clearly seen, as compared to those at the catalyst distance of 0.2 mm.

As shown in Figures 5.10(a)-(f), all product selectivities excepting H_2 vary significantly with respect to the residence time. Both C_2H_2 and C selectivities increased with increasing residence time, but in contrast, the selectivities for C_2H_4, C_2H_6, and C_4H_6 declined markedly. This is due to the fact that at higher residence times, methane molecules have more oppurtunity for being collided by energetic electrons and thus producing more amounts of CH species and C. For the comparative results among three systems, it seems to be no marked differences in all product selectivities. For a comparison between two catalyst distances of 0.2 and 0.5 mm, the selectivity of each product was also comparatively similar. Overall, it can be again concluded that, under the studied experimental conditions, the presence of catalyst had a promotional effect on the methane conversion, but there was no significant effect on the product selectivity. A possible explanation for these results is that the adsorption process of excited species taking place on the catalyst surface is only physisorption, not chemisorption, due to the fact that this studied system was experimentally operated at an ambient temperature without external heating. In other words, the physisorption process generally occurs at relatively low temperatures, while the chemisorption requires high temperatures to activate the process. From the results, it was hypothesized an increase in temperature on the catalyst surface might enhance product selectivities. Therefore, the heating effect of catalyst surface was studied in next investigation.

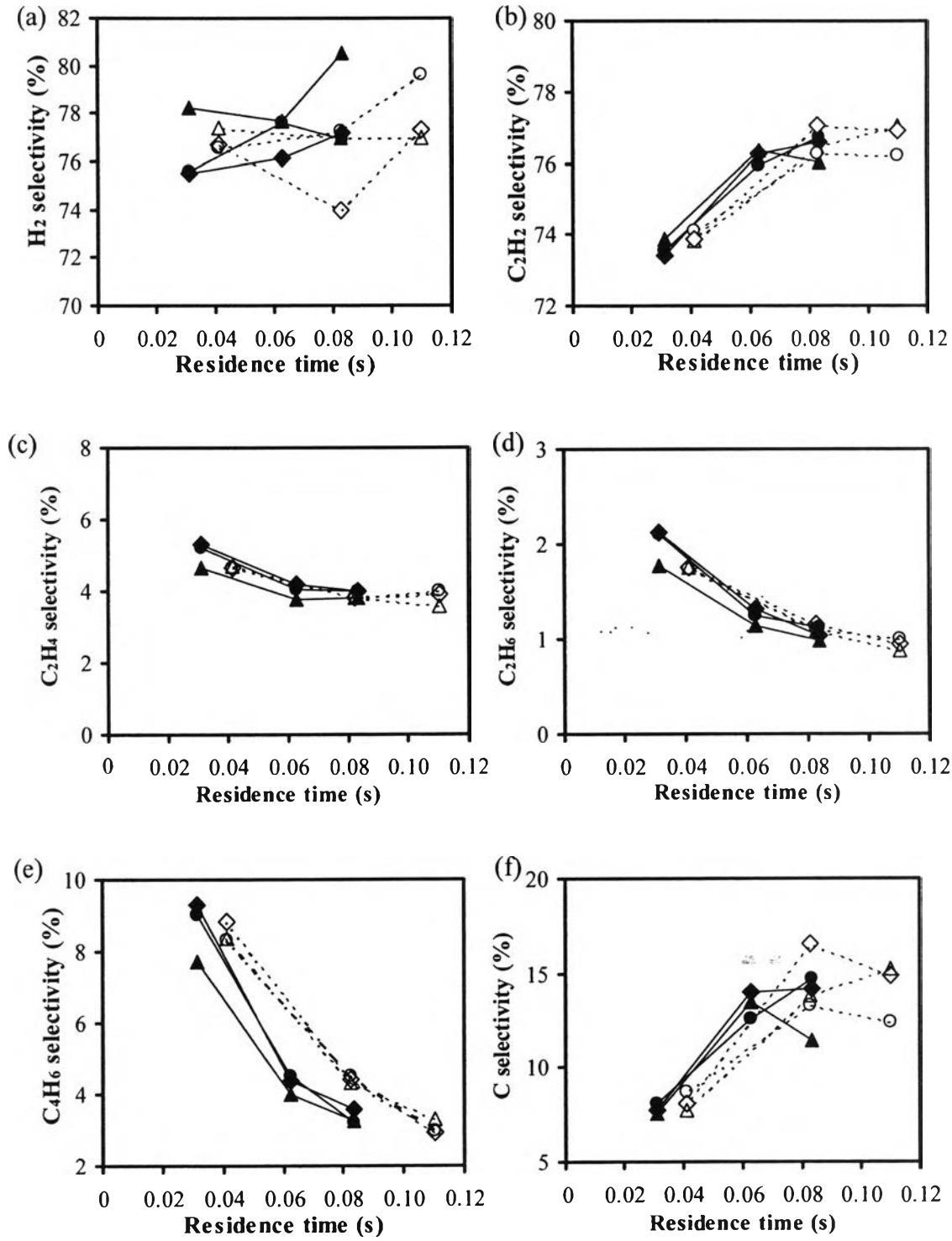

Figure 5.10 Effect of the presence of catalyst on selectivities for (a) H_2, (b) C_2H_2, (c) C_2H_4, (d) C_2H_6, (e) C_4H_6 (1,3-butadiene), and (f) C of the combined catalytic-plasma non-oxidative methane reforming (solid line: catalyst distance of 0.2 mm, dotted line: catalyst distance of 0.5 mm, ▲ and △: plasma alone, ● and ○: plasma+unloaded catalyst, ◆ and ◇: plasma+Ni-loaded catalyst) (CH_4 in feed, 5%; electrode gap distance, 4 mm; and input power, 6 W).

5.4.6 Effect of Catalyst Surface Temperature

To determine whether the temperature of the catalyst surface plays a significant role in improving the overall reaction performance and pathways of the combined plasma-catalytic non-oxidative methane reforming, both unloaded and Ni-loaded porous silica-alumina catalyst plates were heated up to approximately 210°C by using IR beam heater. Moreover, a control experiment of the sole catalyst system with heating (without plasma) was also comparatively carried out. The results showed that the catalytic conversion of methane did not occur in the non-plasma system with the catalyst since this endothermic reaction of non-oxidative methane reforming does not thermodynamically occur at this low temperature of 210°C. Figure 5.11(a) shows the comparative results of methane conversion between all the studied systems with and without heating at the catalyst surface. For the plasma+unloaded catalyst system, the methane conversion was improved when the surface of unloaded catalyst plate was heated up, whereas for the plasma+Ni-loaded catalyst system, the methane conversion slightly increased when the catalyst was heated up to 210°C. Moreover, Figure 5.11(b) and (c) show the comparisons of the H_2 and C_2 yields between the systems with and without heating. As shown in Figure 5.11(b), the heating effect on the H_2 yield has a similar trend to that on the methane conversion. The explanation is that the hydrogen produced is directly derived from the methane conversion. Figure 5.11(c) shows the enhancement of C_2 yield in the plasma+unloaded catalyst system with heating; whereas, in the plasma+Ni-loaded catalyst system, the C_2 yield drastically drops when the surface of Ni-loaded catalyst plate is heated up. These results clearly showed that in the case of unloaded catalyst plate, the heating effect had a significant role in improving both methane conversion and product yields while the heating effect was insignificant for the Ni-loaded catalyst system. The heating effect for the case of unloaded catalyst plate can be explained in that the secondary reactions of methyl radicals might be potentially accelerated by increasing temperature on the surface of catalyst support plate, which contributes to having the higher driving force for the methane dissociation in the initial step, retards the possibilities of backward reactions to recombine to methane, and therefore leads to the enhancement of methane conversion. The role of catalyst surface heating is currently being investigated to obtain a better understanding of the

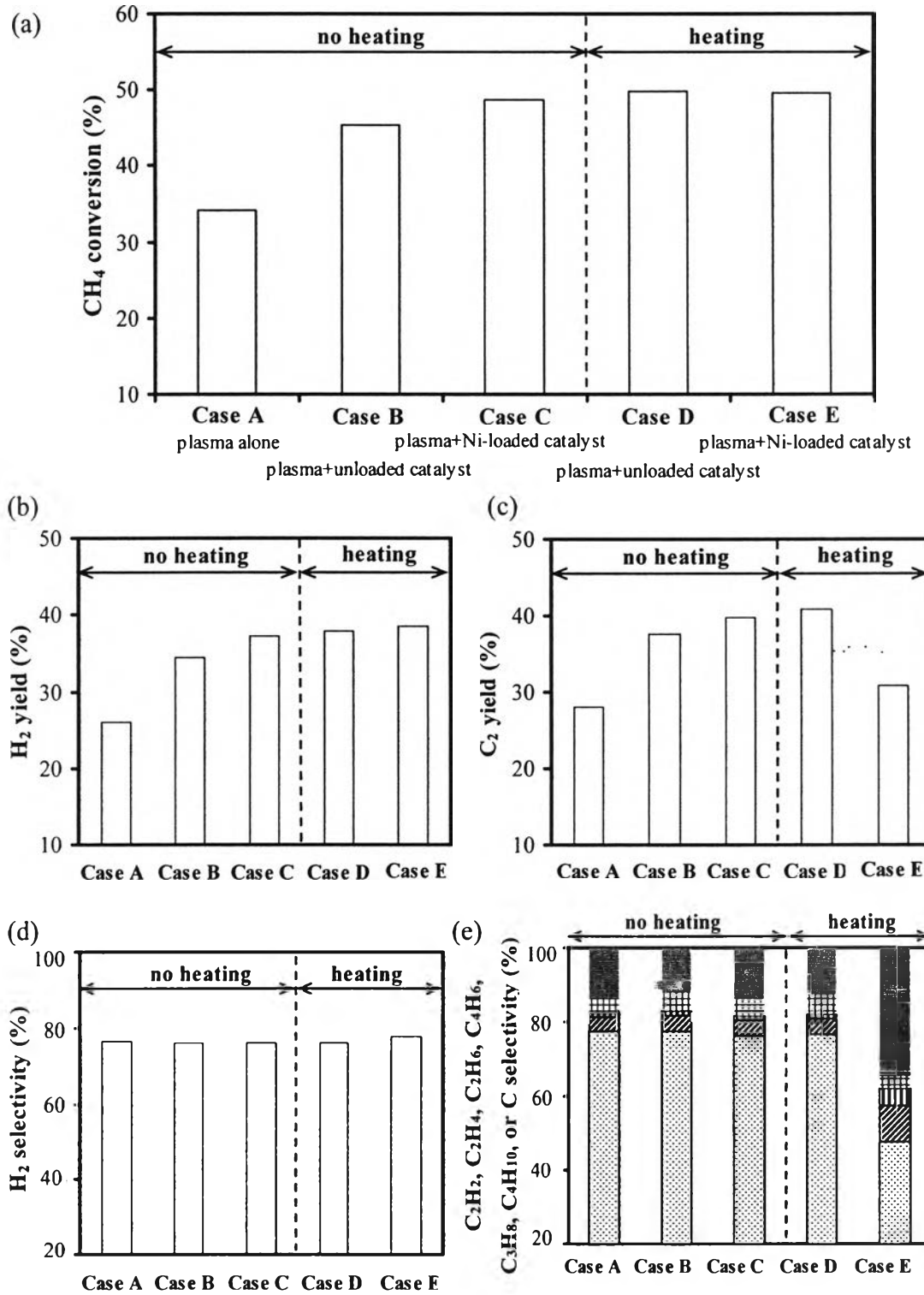

Fig. 11. Effect of catalyst surface temperature on (a) methane conversion (b) H_2 yield, (c) C_2 yield (d) H_2 selectivity, and (e) selectivities for ⊡ C_2H_2, ▨ C_2H_4, ▥ C_2H_6, ▤ 1,3-C_4H_6, ■ C_3H_8+C_4H_{10}, and ▩ C of the combined catalytic-plasma non-oxidative methane reforming (CH_4 in feed, 5%; feed flow rate, 100 cm^3/min; input power, 6 W; electrode gap distance, 4 mm; and, catalyst distance, 0.2 mm).

plasma reforming process. As explained earlier, the increasing temperature up to 210°C is not high enough to promote the endothermic reaction of the non-oxidative methane decomposition. Nonetheless, the dramatic drop of C_2 yield in the plasma+Ni-loaded catalyst system with heating will be discussed below.

Regarding the comparative results of all product selectivities, for all studied systems, the H_2 selectivity is almost the same value of ~76-78%, as shown in Figure 5.11(d). Unlike other product selectivities (C_2H_2, C_2H_4, C_2H_6, C_4H_6, C_3H_8, C_4H_{10}, and C) as shown in Figure 5.11(e), only the plasma+Ni-loaded catalyst system with heating (case E) exhibits the noticeable differences in all the product selectivities while the remaining systems give similar trends for all product selectivities. The selectivities for C_2H_4, C_2H_6, and C in the case E became higher, and those for C_2H_2 and C_4H_6 became less as compared to the other systems. It is clear that the significant decrease in the C_2H_2 selectivity is plausibly the leading cause of the aforementioned drop of C_2 yield. Interestingly, trace amounts of saturated hydrocarbons (C_3H_8 and C_4H_{10}) were found in the plasma+Ni-loaded catalyst system with heating. These results imply that heating the Ni-loaded catalyst possibly causes the chemisorption process of various species on the catalyst surface, and consequently the change in pathways of the plasma-catalytic non-oxidative methane reforming. Both the acetylene cracking ($C_2H_2 \rightarrow 2C + H_2$) and the hydrogenation reactions of various unsaturated hydrocarbons (e.g. C_2H_2, C_2H_4, and C_4H_6) can be potentially activated to occur on the nickel active sites at a temperature of 210°C, which, in turn, led to more tendencies of C, C_2H_4, C_2H_6, C_3H_8 and C_4H_{10} formations. There have been many previous studies reporting that, over nickel-based catalysts, the chemisorbed acetylene can be easily cracked to C and H_2, as well as be hydrogenated to C_2H_4 and C_2H_6 in the temperature range of about 150-250°C [28-30]. Nonetheless, there was no appreciable increase in H_2 selectivity observed, most likely due to the fact that hydrogen from acetylene cracking reaction is partially used for the hydrogenation reactions.

5.5 Proposed Chemical Reaction Pathways for the Non-Oxidative Methane Reforming in the Absence and Presence of Catalyst

To provide a clear understanding of the non-oxidative methane reforming reactions under gliding arc discharge system, it is worth describing all the possibilities of chemical pathways occurring under the studied conditions. Based on the present results, a number of possible reaction pathways involving in both the sole plasma system and the combined plasma and catalyst system are proposed.

5.5.1 Sole Plasma System

In a plasma environment, high energy electrons generated by gliding arc discharge will collide with the gaseous molecules of methane, creating various methyl species, as well as carbon and hydrogen radicals for subsequent reactions (Equations 5.6-5.9).

Electron-methane collisions:

$$e^- + CH_4 \rightarrow CH_3 + H + e^- \quad (5.6)$$

$$e^- + CH_3 \rightarrow CH_2 + H + e^- \quad (5.7)$$

$$e^- + CH_2 \rightarrow CH + H + e^- \quad (5.8)$$

$$e^- + CH \rightarrow C + H + e^- \quad (5.9)$$

The production of C_2 hydrocarbons, including ethane, ethylene, and acetylene, as well as hydrogen molecules is proceeded via the coupling reactions of chemically active species derived from methane dissociations (Equations 5.10-5.16). It is believed that the coupling reactions of either two hydrogen radicals (Equation 5.10) or two CH radicals (Equation 5.16) have more tendency to occur than other coupling reactions, since H_2 and C_2H_2 are the primary products in this studied system.

Coupling reactions of active species:

$$H + H \rightarrow H_2 \quad (5.10)$$

$$CH_3 + CH_3 \rightarrow C_2H_6 \quad (5.11)$$

$$CH_3 + CH_2 + H \rightarrow C_2H_6 \quad (5.12)$$

$$CH_3 + CH \rightarrow C_2H_4 \quad (5.13)$$

$$CH_2 + CH_2 \rightarrow C_2H_4 \quad (5.14)$$

$$CH_2 + CH + H \rightarrow C_2H_4 \quad (5.15)$$

$$CH + CH \rightarrow C_2H_2 \quad (5.16)$$

Furthermore, C_2H_3 radicals can be formed via both the coupling of CH_2 and CH radicals (Equation 5.17), and the coupling of C_2H_2 and H radicals (Equation 5.18), and the coupling of two C_2H_3 radicals are thought to be the dominant reaction for producing butadiene (C_4H_6), as shown in Equation 5.19.

$$CH_2 + CH \rightarrow C_2H_3 \quad (5.17)$$

$$C_2H_2 + H \rightarrow C_2H_3 \quad (5.18)$$

$$C_2H_3 + C_2H_3 \rightarrow C_4H_6 \quad (5.19)$$

Additionally, methane molecules may crack to form carbon residue and hydrogen molecules via thermal cracking reactions, as shown in Equation 5.20. Thermal cracking reaction of methane;

$$CH_4 \rightarrow C + 2H_2 \quad (5.20)$$

5.5.2 Combined Plasma and Catalyst System

In the presence of the studied catalyst, the product distribution of the non-oxidative methane reforming under the studied plasma conditions was found to be noticeably altered with the catalyst surface temperature. This means that the effects of the presence of the nickel catalyst and the catalyst surface temperature have a significant role on the pathways of the plasma-catalytic methane reforming reactions, plausibly by activating the chemisorption process of various excited species on the nickel active sites. According to the aforementioned results of the plasma+Ni-loaded catalyst system with heating, more tendencies of C, C_2H_4, C_2H_6, C_3H_8, and C_4H_{10} formations were observed. A large amount of carbon is thought to be formed from the thermal cracking reaction of acetylene (Equation 5.21) while the C_2H_4, C_2H_6, and C_4H_{10} products are more likely to be produced via the

hydrogenation reactions of unsaturated hydrocarbons (Equations 5.22-5.24) due to the presence of nickel metal behaving as the hydrogenation active site [28-30]. In addition, a very small amount of C_3H_8 is most likely to be formed by coupling reaction of methyl species on the nickel sites (Equation 5.25).

Thermal cracking reaction of acetylene;

$$C_2H_2 \rightarrow 2C + 2H_2 \quad (5.21)$$

Hydrogenation reactions of unsaturated hydrocarbons;

$$C_2H_2 + H_2 \rightarrow C_2H_4 \quad (5.22)$$

$$C_2H_4 + H_2 \rightarrow C_2H_6 \quad (5.23)$$

$$C_4H_6 + 2H_2 \rightarrow C_4H_{10} \quad (5.24)$$

Coupling reaction of methyl species;

$$2CH_3 + CH_2 \rightarrow C_3H_8 \quad (5.25)$$

5.6 Conclusions

In this gliding arc microreactor system under the studied conditions, the dominant products of the direct non-oxidative methane reforming were C_2H_2 and H_2. Input power, discharge gap distance between electrodes, reactor width, and feed flow rate showed the important influences on the methane conversion and product selectivities. The most dominating factor affecting the reaction performance was the residence time. The best improvement of methane conversion, as well as H_2 and C_2 yields, was achieved in the plasma+Ni-loaded catalyst system, as compared to the sole catalyst, sole plasma, and plasma+unloaded catalyst systems. In this plasma microreactor, the distance between catalyst and plasma zone (catalyst distance) or the packing position of catalyst plate was a crucial parameter, which was directly involved in the adsorption-desorption interactions of excited species on the catalyst surface, and therefore the reforming reaction. In addition, the product selectivities were significantly changed when the Ni-loaded catalyst plate was heated to 210°C, possibly due to the fact that the heating effect caused the chemisorption of various excited species on the catalyst surface whereas the heating effect on the methane conversion was insignificant.

5.7 Acknowledgements

The authors thank the Commission on Higher Education, Thailand, the Department of Chemical Engineering, Tokyo Institute of Technology, Japan, the National Research Council of Thailand, the National Excellence Center for Petroleum, Petrochemicals, and Advance Materials under the Ministry of Education, Thailand, and the Research Unit of Petrochemical and Environmental Catalysis under the Ratchadapisek Somphot Endowment Fund, Chulalongkorn University, Thailand.

5.8 References

1. S. Yao, A. Nakayama, E. Suzuki, AIChE J. 47 (2001) 419-426.
2. J. Zhang, Y. Yang, J. Zhang, Q. Liu, K. Tan, Energ. Fuel 16 (2002) 687-693.
3. Y. Yang, Plasma Chem. Plasma Process. 23 (2003) 283-296.
4. L.T. Hsieh, W.J. Lu, C.Y. Chen, M.C. Depew, Appl. Catal. B: Environ. 43 (2003) 187-193.
5. L.N. Misha, K. Shibata, H. Ito, N. Yugami, Y. Nishida, IEEE T. Plasma Sci. 32 (2004) 1727-1733.
6. L.N. Misha, K. Shibata, H. Ito, N. Yugami, Y. Nishida, Surf. Coat. Tech. 201 (2007) 6101-6104.
7. A. Indarto, N. Coowanitwong, J.W. Choi, H. Lee, H.K. Song, Fuel Process. Technol. (2007), In Press.
8. L.M. Zhou, B. Xue, U. Kogelschatz, B. Eliasson, Plasma Chem. Plasma Process. 18 (1998) 375-393.
9. D.D. Tanner, P. Kandanarachchi, Q. Ding, H. Shao, D. Vizitiu, J.A. Franz, Energ. Fuel. 15 (2001) 197-204.
10. D.W. Larkin, L.L. Lobban, R.G. Mallinson, Catal. Today 71 (2001) 199-210.
11. K. Supat, A. Krupong, S. Chavadej, L.L. Lobban, R.G. Mallinson, Energ. Fuel. 17 (2003) 474-481.
12. S. Kado, K. Urasaki, Y. Sekine, K. Fujimoto, T. Nozaki, K. Okazaki, Fuel 82 (2003) 2291-2297.

13. B. Pietruszka, K. Auklam, M. Heintze, Appl. Catal. A: Gen. 261 (2004) 19-24.
14. A. Marafee, C. Liu, G. Xu, R. Mallinson, L. Lobban, Ind. Eng. Chem. Res. 36 (1997) 632-637.
15. G.P. Vissokov, P.S. Pirgov, Appl. Catal. A: Gen. 168 (1998) 229-233.
16. T. Jiang, Y. Li, C.J. Liu, G.H. Xu, B. Eliasson, B. Xue, Catal. Today 72 (2002) 229-235.
17. M.T. Radoin, Y. Chen, M.C. Depew, Appl. Catal. B: Environ. 43 (2003) 187-193.
18. B. Pietruszka, M. Heintze, Catal. Today 90 (2004) 151-158.
19. Istadi, N.A.S. Amin, Fuel 85 (2006) 577-592.
20. T. Nozaki, A. Hattori, K. Okazaki, Catal. Today 98 (2004) 607-616.
21. J.C. Ganley, E.G. Seebauer, R.I. Masel, AIChE J. 50 (2004) 829-834.
22. I. Aartun, T. Gjervan, H. Venvik, O. Görke, P. Pfeifer, M. Fathi, A. Holmen, K. Schubert, Chem. Eng. J. 101 (2004) 93-99.
23. H. Sekiguchi, M. Audo, H. Kojima, J. Phys. D: Appl. Phys. 38 (2005) 1722-1727.
24. A. Yamamoto, S. Mori, M. Suzuki, Thin Solid Films 515 (2007) 4296-4300.
25. S. Suzuki, H. Sekiguchi, K. Takaki, J. Chem. Eng. Jpn. 40 (2007) 749-754.
26. H. Löwe, W. Ehrfeld, Electrochim. Acta 44 (1999) 3679-3689.
27. O. Wörz, K.P. Jäckel, Th. Richter, A. Wolf, Chem. Eng. Sci. 56 (2001) 1029-1033.
28. J.A. Peña, J. Herguido, C. Guimon, A. Monzón, J.Santamaría, J. Catal. 159 (1996) 313-322.
29. J.W. Medlin, M.D. Allendorf, J. Phys. Chem. B 107 (2003) 217-223.
30. L. Yu, Y. Qin, Z. Cui, Mater. Lett. 59 (2005) 459-462.